Journal of Molecular Structure 1115 (2016) 94–104

Contents lists available at ScienceDirect

Journal of Molecular Structure

journal homepage: http://www.elsevier.com/locate/molstruc

Synthesis, vibrational spectroscopic investigations, molecular docking, antibacterial and antimicrobial studies of 5-ethylsulphonyl-2-(p-aminophenyl)benzoxazole

Shana Parveen S [a], Monirah A. Al-Alshaikh [b], C.Yohannan Panicker [a, c, *], Ali A. El-Emam [d], Mustafa Arisoy [e], Ozlem Temiz-Arpaci [e], C. Van Alsenoy [f]

[a] Department of Physics, TKM College of Arts and Science, Kollam, Kerala, India
[b] Department of Chemistry, College of Science, King Saud University, Riyadh, 11451, Saudi Arabia
[c] Department of Physics, Fatima Mata National College, Kollam, Kerala, India
[d] Department of Pharmaceutical Chemistry, College of Pharmacy, King Saud University, Riyadh, 11451, Saudi Arabia
[e] Department of Pharmaceutical Chemistry, Ankara University, TR-06100, Tandogan, Ankara, Turkey
[f] Department of Chemistry, University of Antwerp, Groenenborgerlaan 171, B-2020, Antwerp, Belgium

ARTICLE INFO

Article history:
Received 9 January 2016
Received in revised form
15 February 2016
Accepted 15 February 2016
Available online 23 February 2016

Keywords:
DFT
Benzoxazole
IR
Raman
Molecular docking

ABSTRACT

The optimized molecular structure, vibrational wavenumbers, corresponding vibrational assignments of 5-ethylsulphonyl-2-(p-aminophenyl)benzoxazole have been investigated experimentally and theoretically based on density functional theory. Synthesis and antibacterial and antimicrobial activities of the title compound were reported. The FT-IR and FT-Raman spectra were recorded in solid phase and the experimental bands were assigned and characterized on the basis of potential energy distribution. The HOMO and LUMO energies show that the charge transfer occur within the molecule. Stability arising from hyperconjugative interactions and charge delocalization were analysed using natural bond orbital analysis. Binding free energy of −9.8 kcal/mol as predicted by docking studies suggests good binding affinity and the inhibitor forms a stable complex with FAK as is evident from the ligand−receptor interactions. The title compound possesses lower activity against *Candida albicans* with MIC value of 64 μg/ml than the compared reference drugs as fluconazole and amphotericin B and possesses the same activity with value of 64 μg/ml against *Candida krusei* as the reference drug, fluconazole.

1. Introduction

Benzoxazole derivatives show various biological activities and exhibit chemotherapeutic activities [1,2]. Benzoxazole derivatives exhibit antimicrobial [3–5], antiviral [6,7], multi-drug resistance cancer cell activities [8], with inhibitory activity on eukaryotic topoisomerase II enzyme in cell-free system [9–11]. Recently Anusha and Rao [12] reported the synthesis and biological evaluation of benzoxazole derivatives as new antimicrobial agents. Mary et al. reported the vibrational spectroscopic and SERS studies of some benzoxazole derivatives [13,14]. Literature survey reveals that so far there is no complete experimental and theoretical study of the title compound. In the present study, both experimental and theoretical analysis are combined for studying the optimized molecular structural parameters, vibrational spectra, first and second order hyperpolarizabilities and HOMO-LUMO energies for the title compound using DFT/B3LYP method using 6-311++G(d,p) (5D, 7F). Synthesis, antibacterial and antimicrobial activities and the molecular docking study are also reported.

2. Experimental details

The chemicals and solvents were purchased from Sigma−Aldrich Co. (Taufkirchen, Munich Germany) and Fisher Scientific (Pittsburgh, PA, USA) and were used without purification. Silica gel HF_{254} chromatoplates (0.3 mm) were used for TLC and the mobile phase was chloroform/methanol (10:0.5) for compound **1**. Melting point was recorded on a Stuart Scientific SMP 1 (Bibby Scientific Limited, Staffordshire, UK) instrument and is uncorrected. The FT-IR spectrum (Fig. 1) was recorded using KBr pellets on a DR/Jasco FT-IR

* Corresponding author. Department of Physics, TKM College of Arts and Science, Kollam, Kerala, India.
E-mail address: cyphyp@rediffmail.com (C.Yohannan Panicker).

http://dx.doi.org/10.1016/j.molstruc.2016.02.057
0022-2860/

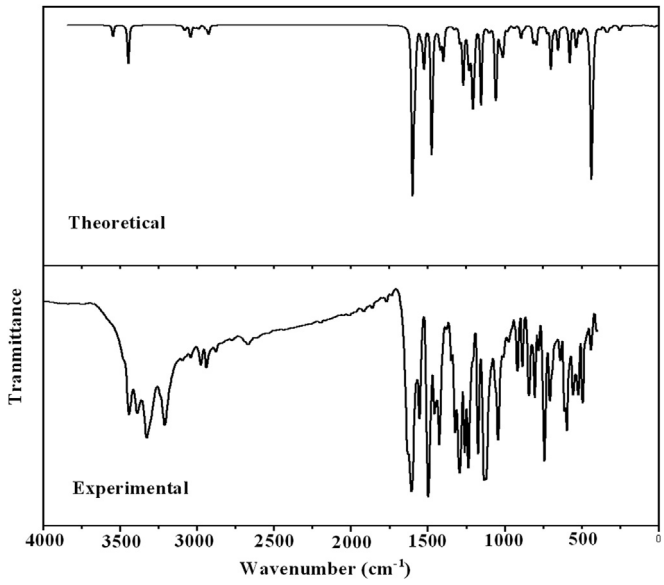

Fig. 1. FT-IR spectrum of 5-Ethylsulphonyl-2-(p-aminophenyl)benzoxazole.

6300 spectrometer. The FT-Raman spectrum (Fig. 2) was obtained on a Bruker RFS100/S FT-Raman spectrometer (Nd:YAG laser, 1064 nm excitation). NMR spectra were recorded on a Varian Mercury 400 MHz NMR spectrometer (Palo Alto, CA, USA) in $CDCl_3$ or dimethylsulfoxide (DMSO-d_6); tetramethylsilane (TMS) was used as an internal standard. The mass spectra were recorded on a Waters ZQ Micromass LC-MS spectrometer (Milford, MA, USA) using the ESI(+) method. Elemental analysis was performed on an LECO 932 CHNS (St. Joseph, MI, USA) instrument and was within ±0.4% of theoretical value.

Materials used in the microbiology study were; Mueller Hinton Agar (MHA) (Merck), Mueller Hinton Broth (MHB) (Merck), Sabouraud Dextrose Agar (SDA) (Merck), RPMI–1640 medium with L-glutamine (Sigma), 3-[N-morpholino]-propane-sulphonic acid (MOPS) (Sigma), 96-well microplates (Falcon), Transfer pipette (Eppendorf), ampicillin (Mustafa Nevzat Pharmaceuticals),

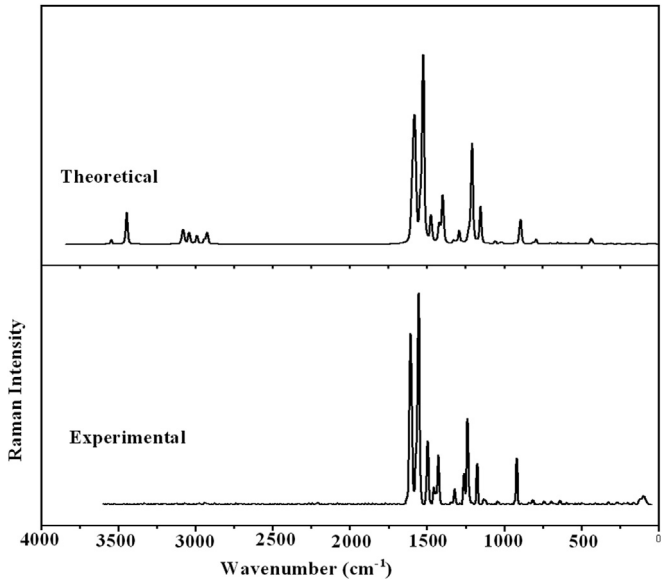

Fig. 2. FT-Raman spectrum of 5-Ethylsulphonyl-2-(p-aminophenyl)benzoxazole.

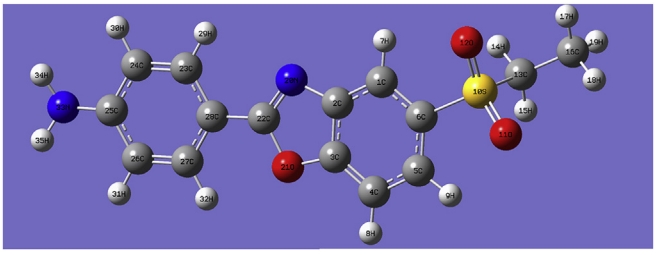

Fig. 3. Optimized geometry of 5-Ethylsulphonyl-2-(p-aminophenyl)benzoxazole.

gentamycin sulphate (Paninkret Chem.-Pharm.), ofloxacin (Zhejiang Huangyan East Asia Chemical CO. Ltd.), meropenem (Astra Zeneca), ceftriaxone (Mustafa Nevzat Pharmaceuticals), tetracycline (Mustafa Nevzat Pharmaceuticals), fluconazole (Sigma), amphotericin B trihydrate (Bristol Myers Squibb), DMSO (Riedel de Haen). Isolates were *Escherichia coli* isolate (has Extended Spectrum Beta Lactamase (ESBL) enzyme), *Enterococcus faecalis* isolate (resistant to vancomycin (VRE)), *Pseudomonas aeruginosa* isolate (resistant to gentamycin) and *Staphylococcus aureus* isolate ([resistant to methicillin (MRSA)). Standard strains were; *E. coli* ATCC 25922, *E. faecalis* ATCC 29212, *P. aeruginosa* ATCC 27853, *S. aureus* ATCC 29213, *Candida albicans* ATCC 10231, *Candida krusei* ATCC 6258.

3. General for the preparation of compound 1

5-Ethylsulphonyl-2-(p-amino-phenyl)benzoxazole (**1**) was synthesized by heating 0.01 mol 4-ethylsulphonyl-2-aminophenol. HCl with 0.01 mol p-amino-benzoic acid in 24 g polyphosphoric acid was stirred 3 h. At the end of the rection period, the residue was poured into ice-water, stirred and was neutralized with excess of 10% NaOH solution extracted with benzene. The benzene solution was dried over anhydrous sodium sulphate and evaporated under diminished pressure. The residue was boiled with 200 mg charcoal in ethanol and filtered. After the evaporation of solvent *in vacuo*, the crude product was obtained and recrystallized from ethanol-water mixture and compound **1** was dried *in vacuo* [15]. The chemical, physical and spectral data of the compound **1** are: yield: 64.83%, M.p. 206 °C, 1H NMR (δ in ppm, J in Hz) 8.144–8.139 (s, 1H, J = 2.0 Hz), 7.950–7.905 (m, 3H), 8.850–7.824 (dd, 1H, J4 = 1.6 Hz, J = 8.8 Hz), 6.746–6.725 (d, 2H, J = 8.4 Hz), 6.185 (s,2H), 3.398–3.343 (q, 2H), 1.133 (t,3H); MS (ESI^+) *m/z* (%) (M + H): (100%), 303.7 (M^++H).

4. Microbiological assays

For microbiological assays, standard powders of ampicillin, gentamycin sulphate, ofloxacin, vancomycin, fluconazole, and amphotericin B trihydrate were dissolved in appropriate solvents recommended by Clinical and Laboratory Standards Institute (CLSI) guidelines [16,17]. Stock solutions of the test compounds were prepared in DMSO. Bacterial susceptibility testing was performed according to the guidelines of CLSI M100-S18 [17]. MHB was added to each well of the microplates. The bacterial suspensions used for inoculation were prepared at 10^5 CFU/ml by diluting fresh cultures at McFarland 0.5 density (10^7 CFU/ml). Suspensions of the bacteria at 10^5 CFU/ml were inoculated to the two-fold diluted solution of the compounds. A 10-μl bacteria inoculum was added to each well of the microplates. There were 10^4 CFU/ml bacteria in the wells after inoculations. Microplates were incubated at 37 °C overnight. Also fungal susceptibility testing was performed according to the guidelines of CLSI M27-A3 [16]. RPMI-1640 medium with L-

glutamine buffered to pH 7 with MOPS was added to each well of the microplates. The colonies were suspended in sterile saline, and the resulting suspension was adjusted to McFarland 0.5 density (10^6 CFU/ml). A working suspension was prepared by a 1:100 dilution followed by a 1:20 dilution of the stock suspension. 10 μl of this suspension at 10^3 CFU/ml were inoculated to the two-fold diluted solution of the compounds. Microplates were incubated at 35 °C for 24–48 h. After incubation, the lowest concentration of the compounds that completely inhibited macroscopic growth was determined and reported as minimum inhibitory concentration (MIC: μg/ml). All solvents and diluents, pure microorganisms and pure media were used in control wells. All experiments were done in 3 parallel series.

5. Computational details

Calculations of the title compound were carried out with Gaussian09 software [18] using B3LYP/6-311++G(d,p) (5D, 7F) basis set to predict the molecular structure and vibrational wavenumbers. This basis set was chosen particularly because of its advantage of doing faster calculations with relatively better accuracy and structures and it contains both soft and polarisation functions and it has proven to yield reliable descriptions of the molecular structure [19,20]. As the DFT hybrid B3LYP functional tends to overestimate the wavenumbers of the fundamental modes, a scaling factor of 0.9613 has been uniformly applied to the calculated wavenumbers [21]. The assignments of the calculated wavenumbers are aided by the animation option of GAUSSVIEW program [22] and potential energy distribution by GAR2PED software package [23]. The theoretically optimized geometrical parameters are given in Table 1.

6. Results and discussion

6.1. Antibacterial and antimicrobial activities

The synthesis of the 5-ethylsulphonyl-2-(p-aminophenyl)benzoxazole (**1**) was obtained by heating p-aminobenzoic acid with 4-ethylsulphonyl-2-aminophenol in PPA (polyphosphoric acid) as the cyclodehydration reagent in a one step procedure [15]. The synthesis is shown in Scheme 1. Structure of its was supported by spectral data. The IR, ^{1}H NMR and Mass spectra are in agreement with the proposed structures.

The compound **1** was assayed in vitro for antibacterial activity against *P. aeruginosa* ATCC 25853, *E. coli* ATCC 25922, *P. aeruginosa* isolate (resistant to gentamicin), *E. coli* isolate (resistant to ESBL) as Gram-negative bacteria, *E. faecalis* ATCC 29212; *S. aureus* ATCC 29213, *E. faecalis* isolate (resistant to vancomycin), *S. aureus* isolate (resistant to methicillin) as Gram-positive bacteria and the antifungal activity was evaluated against *C. albicans* ATCC 10231 and *C. krusei* ATCC 6258. The MIC values were determined by two fold serial dilution technique in Mueller-Hinton broth and Sabouraud Dextrose agar for the antibacterial and antifungal assay, respectively. For comparison of the antimicrobial activity, meropenem, ampicillin trihydrate, gentamycin sulphate, ceftriaxone, tetracycline, ofloxacine were used as the reference antibacterial agents and fluconazole, amphotericin B were employed as the reference antifungal agents. All the biological results of the tested compound are given in Table 2.

In this study, our goal was to investigate the role of efficience substitution on the two positions with a p-aminophenyl group of 5-ethylsulphonyl-benzoxazole ring for antimicrobial activity. The compound 1 indicated a broad antibacterial activity against some *E. coli, P. aeruginosa* and their isolates as Gram-negative bacteria possessing MIC values between 128 and 64 μg/ml. The compound 1 was less active than the compared reference drugs against these Gram-negative bacteria. Also compound 1 showed a broad antibacterial activity against some *S. aureus, E. faecalis* and their isolates with a 128–64 μg/ml. MIC values. It displayed the same activity reference drugs: ampicillin, gentamycin sulphate and ceftriaxone against MRSA.

The tested compound 1 possessed lower activity against *C. albicans* with MIC value of 64 μg/ml than compared reference drugs as fluconazole and amphotericin B. On the other hand, it possessed the same activity with value of 64 μg/ml against *C. krusei* as the reference drug, fluconazole.

6.2. IR and Raman spectra

The observed IR, Raman bands and calculated (scaled) wavenumbers with assignments are given in Table 3. In the following discussion, the 1–4-disubstituted phenyl ring, 1,2,4-trisubstituted phenyl ring and benzoxazole ring are designated as PhI, PhII and PhIII, respectively.

The N–H stretching vibration occurs in the region 3300–3500 cm^{-1} and for the title compound, the NH_2 stretching modes are assigned at 3446 (IR), 3505, 3464 (Raman) and at 3546, 3446 cm^{-1} theoretically [24]. The NH_2 in-plane bending vibrations expected [24] around 1650 cm^{-1} and in the present case, the bands at 1603 cm^{-1} in the IR spectrum, 1608 cm^{-1} in the Raman spectrum and at 1601 cm^{-1} theoretically are assigned as the NH_2 in-plane bending vibration. According to Roeges [24] the rocking mode of NH_2 is expected in the range 1120–1020 cm^{-1} and in the present case the bands observed at 1035 cm^{-1} in the IR spectrum and at 1031 (DFT) are assigned as this mode. For the title compound the wagging mode of NH_2 is observed at 633 cm^{-1} in IR, 635 cm^{-1} in Raman and at 631 cm^{-1} theoretically, which is in agreement with the literature [24].

The stretching vibrations of the CH_2 group appears in the range 3020–2875 cm^{-1} [24,25] and for the title compound, the CH_2 stretching modes are observed at 2942 cm^{-1} in the IR spectrum, 2940 cm^{-1} in the Raman spectrum and at 2992, 2944 cm^{-1} theoretically. The deformation modes of CH_2 are assigned at 1399, 1251, 1198 and 758 cm^{-1} theoretically as expected [24]. The stretching vibrations of CH_3 are expected in the range 3050–2900 cm^{-1} [24,25] and the bands at 2980 cm^{-1} in the IR spectrum, 2978 cm^{-1} in the Raman spectrum and 3011, 2988, 2925 cm^{-1} theoretically are assigned as the stretching modes of the methyl group of the title compound. The deformation modes of the methyl group are expected in the range 1485–1355 cm^{-1} [24] and in the present case these modes are assigned at 1355 (IR) and 1449, 1434, 1358 cm^{-1} theoretically. Aromatic molecules display a methyl rock in the neighbourhood 1045 cm^{-1} and another one in the region 970 ± 70 cm^{-1} [24] and these modes are assigned at 1026 and 1016 cm^{-1} theoretically. The methyl torsions [24] are often assigned in the region 185 ± 65 cm^{-1}.

Normally the sulphur compounds show peaks in the region 1360–1210 and 1165–1135 [24] due to the S=O asymmetric and symmetric stretching vibrations. For the title compound, the DFT calculations give these modes at 1237 and 1198 cm^{-1}. The asymmetric SO_2 stretching mode is observed at 1236 cm^{-1} in the IR spectrum and at 1240 cm^{-1} in the Raman spectrum. The deformation modes of SO_2 are expected in the regions, 535 ± 40, 485 ± 50, 405 ± 65 and 320 ± 40 cm^{-1} [24] and in the present case, these bands are observed at 566, 455 cm^{-1} in the IR spectrum, 448 cm^{-1} in the Raman spectrum and at 577, 451, 379, 308 cm^{-1} theoretically. The SO_2 deformation modes are reported at 575, 457, 390 and 298 cm^{-1} theoretically for a similar derivative [13]. The C–S stretching modes are assigned at 655 and 699 cm^{-1} theoretically as expected [24] and the reported values are 704 and

Table 1
Optimized geometrical (B3LYP) parameters of 5-Ethylsulphonyl-2-(p-aminophenyl)benzoxazole atom labelling according to Fig. 3. Bond lengths (Å).

Bond lengths (Å)					
C1–C2	1.3933	C1–C6	1.3938	C1–H7	1.0823
C2–C3	1.4026	C2–N20	1.3882	C3–C4	1.3838
C3–O21	1.3653	C4–C5	1.3948	C4–H8	1.0823
C5–C6	1.4031	C5–H9	1.0826	C6–S10	1.8041
S10–O11	1.4702	S10–O12	1.4695	S10–C13	1.8274
C13–H14	1.0917	C13–H15	1.0917	C13–C16	1.5257
C16–H17	1.0912	C16–H18	1.0912	C16–H19	1.0927
N20–C22	1.2988	O21–C22	1.3871	C22–C28	1.4496
C23–C24	1.3824	C23–C28	1.4049	C23–H29	1.083
C24–C25	1.4078	C24–H30	1.085	C25–C26	1.4059
C25–N33	1.3838	C26–C27	1.3849	C26–H31	1.0849
C27–C28	1.4034	C27–H32	1.0827	N33–H34	1.0081
N33–H35	1.0081				
Bond angles (°)					
C2–C1–C6	116.4	C2–C1–H7	122.1	C6–C1–H7	121.5
C1–C2–C3	119.9	C1–C2–N20	131.4	C3–C2–N20	108.8
C2–C3–C4	124.1	C2–C3–O21	107.4	C4–C3–O21	128.5
C3–C4–C5	116.0	C3–C4–H8	122.2	C5–C4–H8	121.8
C4–C5–C6	120.4	C4–C5–H9	120.5	C6–C5–H9	119.1
C1–C6–C5	123.2	C1–C6–S10	118.4	C5–C6–S10	118.3
C6–S10–O11	108.0	C6–S10–O12	108.1	C6–S10–C13	103.8
O11–S10–O12	120.6	O11–S10–C13	107.6	O12–S10–C13	107.5
S10–C13–H14	105.8	S10–C13–H15	105.8	S10–C13–C16	110.7
H14–C13–H15	109.3	H14–C13–C16	112.4	H15–C13–C16	112.5
C13–C16–H17	111.0	C13–C16–H18	111.0	C13–C16–H19	109.3
H17–C16–H18	108.7	H17–C16–H19	108.4	H18–C16–H19	108.4
C2–N20–C22	105.0	C3–O21–C22	104.5	N20–C22–O21	114.3
N20–C22–C28	128.3	O21–C22–C28	117.4	C24–C23–C28	120.8
C24–C23–H29	120.3	C28–C23–H29	118.9	C23–C24–C25	120.7
C23–C24–H30	119.8	C25–C24–H30	119.5	C24–C25–C26	118.5
C24–C25–N33	120.7	C26–C25–N33	120.8	C25–C26–C27	120.7
C25–C26–H31	119.6	C27–C26–H31	119.8	C26–C27–C28	120.8
C26–C27–H32	119.6	C28–C27–H32	119.7	C22–C28–C23	119.6
C22–C28–C27	121.8	C23–C28–C27	118.6	C25–N33–H34	117.4
C25–N33–H35	117.5	H34–N33–H35	114.0		
Dihedral angles (°)					
C6–C1–C2–C3	0.4	C6–C1–C2–N20	179.8	H7–C1–C2–C3	−178.1
H7–C1–C2–N20	1.2	C2–C1–C6–C5	−0.7	C2–C1–C6–S10	178.7
H7–C1–C6–C5	177.8	H7–C1–C6–S10	−2.7	C1–C2–C3–C4	0.2
C1–C2–C3–O21	179.6	N20–C2–C3–C4	−179.3	N20–C2–C3–O21	0.1
C1–C2–N20–C22	−179.5	C3–C2–N20–C22	−0.1	C2–C3–C4–C5	−0.5
C2–C3–C4–H8	178.9	O21–C3–C4–C5	−179.7	O21–C3–C4–H8	−0.4
C2–C3–O21–C22	−0.0	C4–C3–O21–C22	179.3	C3–C4–C5–C6	0.1
C3–C4–C5–H9	178.4	H8–C4–C5–C6	−179.2	H8–C4–C5–H9	−1.0
C4–C5–C6–C1	0.5	C4–C5–C6–S10	−179.0	H9–C5–C6–C1	−177.8
H9–C5–C6–S10	2.8	C1–C6–S10–O11	157.4	C1–C6–S10–O12	25.4
C1–C6–S10–C13	−88.6	C5–C6–S10–O11	−23.1	C5–C6–S10–O12	−155.1
C5–C6–S10–C13	90.9	C6–S10–C13–H14	57.7	C6–S10–C13–H15	−58.2
C6–S10–C13–C16	179.7	O11–S10–C13–H14	172.0	O11–S10–C13–H15	56.1
O11–S10–C13–C16	−66.0	O12–S10–C13–H14	−56.7	O12–S10–C13–H15	−172.6
O12–S10–C13–C16	65.3	S10–C13–C16–H17	−60.5	S10–C13–C16–H18	60.5
S10–C13–C16–H19	−180.0	H14–C13–C16–H17	57.5	H14–C13–C16–H18	178.5
H14–C13–C16–H19	−61.9	H15–C13–C16–H17	−178.5	H15–C13–C16–H18	−57.5
H15–C13–C16–H19	62.0	C2–N20–C22–O21	0.0	C2–N20–C22–C28	−179.9
C3–O21–C22–N20	0.0	C3–O21–C22–C28	180.0	N20–C22–C28–C23	−0.2
N20–C22–C28–C27	179.9	O21–C22–C28–C23	179.8	O21–C22–C28–C27	−0.0
C28–C23–C24–C25	0.1	C28–C23–C24–H30	−179.8	H29–C23–C24–C25	−179.8
H29–C23–C24–H30	0.4	C24–C23–C28–C22	−179.8	C24–C23–C28–C27	0.0
H29–C23–C28–C22	0.0	H29–C23–C28–C27	179.9	C23–C24–C25–C26	−0.1
C23–C24–C25–N33	−177.7	H30–C24–C25–C26	179.7	H30–C24–C25–N33	2.1
C24–C25–C26–C27	0.1	C24–C25–C26–H31	−179.7	N33–C25–C26–C27	177.7
N33–C25–C26–H31	−2.1	C24–C25–N33–H34	−20.3	C24–C25–N33–H35	−162.2
C26–C25–N33–H34	162.1	C26–C25–N33–H35	20.3	C25–C26–C27–C28	−0.1
C25–C26–C27–H32	179.8	H31–C26–C27–C28	179.8	H31–C26–C27–H32	−0.3
C26–C27–C28–C22	179.8	C26–C27–C28–C23	−0.0	H32–C27–C28–C22	−0.0
H32–C27–C28–C23	−179.9				

663 cm^{-1} for a similar derivative [13].

The COC stretching modes are observed at 1173, 890 cm^{-1} in the IR spectrum, 1174, 888 cm^{-1} in the Raman spectrum and at 1172, 893 cm^{-1} theoretically as expected [26,27]. For the title compound, the CN stretching modes are assigned at 1211 cm^{-1} in the IR, 1208 cm^{-1} in Raman and at 1270, 1209 cm^{-1} theoretically. Bhagyasree et al. [26] reported CN stretching modes at 1247 and 1236 cm^{-1} and Mary et al. [14] reported the CN stretching modes at 1233, 1209 cm^{-1} (DFT), 1238 cm^{-1} (Raman) for a similar benzoxazole derivatives. The C=N stretching mode is expected in the

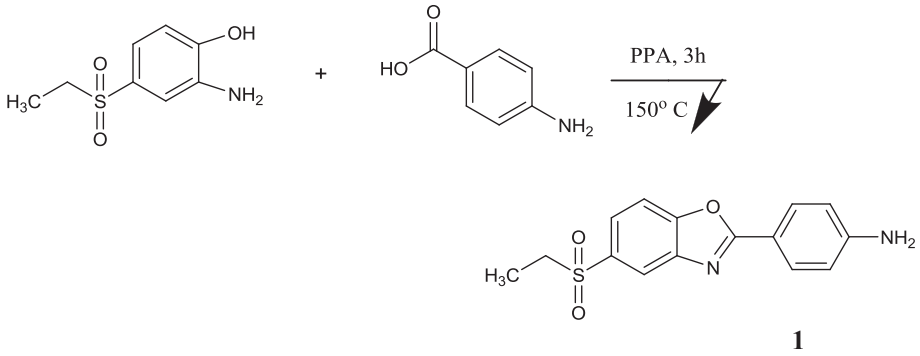

Scheme 1. Pathway of the synthesized compound 1.

Table 2
Antimicrobial activity results (MIC μg/ml) of synthesized compound (1) with the standard drugs.

Compound	S.a.	S.a.*	E.f.	E.f.*	E.c.	E.c.*	P.a.	P.a.*	C.a.	C.k.
1 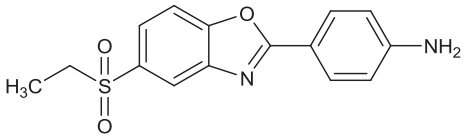	128	64	128	128	128	128	64	64	64	64
Meropenem	<2	<2	<2	8	<2	<2	8	8		
Ampicillin trihydrate	8	64	–	–	<2	32	<2	4		
Ceftriaxone	<2	64	16	32	8	64	–	–		
Gentamycin	<2	64	<2	32	<2	64	4	4		
Tetracycline	<2	64	16	32	1	32	2	64		
Ofloxacin	<2	16	<2	32	<2	<2	<2	<2		
Fluconazole									1	64
Amphotericin B									<0.25	0.5

S.a.: *Staphylococcus aureus* ATCC 29213; S.a.*: *Staphylococcus aureus* isolated (MRSA); E.f.: *Enterococcus faecalis* ATCC 29212; E.f.*: *Enterococcus faecalis* isolated (VRE); E.c.: *Escherichia coli* ATCC 25922; E.c.*: *Escherichia coli* isolated (ESBL); P.a.: *Pseudomonas aeruginosa* ATCC 27853; P.a.*: *Pseudomonas aeruginosa* isolated (gentamycin resistant); *C.a.: Candida albicans* ATCC 10231; *C.k.: Candida krusei* ATCC 6258.

range 1670–1500 cm^{-1} [27,28] and in the present case, this mode is assigned at 1515 cm^{-1} in the IR spectrum and at 1526 cm^{-1} theoretically. Mary et al. [14] reported the C=N stretching mode at 1523 cm^{-1} (IR), 1522 cm^{-1} (Raman) and at 1536 cm^{-1} theoretically for a benzoxazole derivative. For the title compound, the C–C stretching modes are assigned at 1026 and 940 cm^{-1} theoretically and these modes contain contributions from other modes also [29].

The aromatic CH stretching vibrations [24] absorb between 3120 and 3000 cm^{-1}. The B3LYP calculations give bands in the range 3077–3041 cm^{-1} and 3086–3074 cm^{-1} as CH stretching modes of the phenyl rings, PhI and PhII, respectively. Experimentally, we have observed bands at 3088, 3038 cm^{-1} in the IR spectrum and at 3102, 3072, 3035 cm^{-1} in the Raman spectrum as υCH modes. The ring breathing mode for the para substituted benzenes with entirely different substituent [30] is expected in the region 780–840 cm^{-1} and for the title compound this is confirmed by the band in the IR spectrum at 788 cm^{-1}, which finds support from the computational result at 792 cm^{-1}. The ring breathing mode of para-substituted benzenes were reported at 804 and 792 cm^{-1} experimentally and at 782 and 795 cm^{-1} theoretically [31,32]. In asymmetric tri-substituted benzenes, when all the three substituents are heavy, the wavenumber appears [30] at around 1100 cm^{-1} and for or the title compound the phenyl ring II breathing mode is assigned at 1098 cm^{-1} theoretically. The phenyl ring stretching modes are observed at 1550, 1469 cm^{-1} (IR), 1550, 1467 cm^{-1} (Raman) for PhI and at 1571, 1515, 1425, 1326 cm^{-1} (IR), 1426, 1326 cm^{-1} (Raman) for PhII. The DFT calculations give these modes in the ranges 1588–1310 cm^{-1} and 1575–1328 cm^{-1} for PhI and PhII, respectively. For para-substituted benzenes, the in-plane CH bending modes are seen in the range 995–1315 cm^{-1} and for tri-substituted benzenes these modes are in the range [24] 1290–1050 cm^{-1}. In the present case, these in-plane CH bending modes are observed at 1294, 1145, 1115, 1035 cm^{-1} in the IR spectrum and at 1288, 1148 cm^{-1} in the Raman spectrum for PhI and at 1173 cm^{-1} in IR and 1174 cm^{-1} in Raman spectrum for PhII. The B3LYP calculations give these modes in the range 1031–1291 cm^{-1} for PhI and 1098–1228 cm^{-1} for PhII. The out-of-plane CH deformations [24] are observed between 700 and 1000 cm^{-1} and for the title compound, these out-of-plane CH modes are observed at 947, 820, 808 cm^{-1} (IR), 820 cm^{-1} (Raman) and 922 cm^{-1} (IR), 920 cm^{-1} (Raman) for PhI and PhII rings. The DFT calculations give these modes in the range 811–945 cm^{-1} for PhI and 797–925 cm^{-1} for PhII rings.

6.3. Natural bond orbital analysis

The natural bond orbital (NBO) calculations were performed using NBO 3.1 program [33] as implemented in the Gaussian09 package at the DFT/B3LYP level. The possible intensive interactions are given in Table 4. The important intra-molecular hyper conjugative interactions are that of: S_{10}–O_{12} from O_{11} of $n_3(O_{11})$ → $\sigma^*(S_{10}–O_{12})$, S_{10}–O_{11} from O_{12} of $n_3(O_{12})$→$\sigma^*(S_{10}–O_{11})$, O_{21}–C_{22} from N_{20} of $n_1(N_{20})$→ $\sigma^*(O_{21}–C_{22})$, N_{20}–C_{22} from O_{21} of $n_2(O_{21})$→ $\pi^*(N_{20}–C_{22})$, N_{20}–C_{22} from C_{28} of $n_1(C_{28})$→ $\pi^*(N_{20}–C_{22})$, with electron densities, 0.14669, 0.14715, 0.06464, 0.31817, 0.31817e and stabilization energies 22.80, 22.87, 14.48, 32.94, 79.88 kJ/mol.

The bonding in terms of the natural hybrid orbitals with higher energies and considerable p-character are: $n_3(O_{11})$, $n_3(O_{12})$, $n_2(O_{21})$,

Table 3
Calculated (scaled) wavenumbers, observed IR, Raman bands and assignments of 5-Ethylsulphonyl-2-(p-aminophenyl)benzoxazole.

B3LYP/6-311++G(d,p) (5D, 7F)			IR	Raman	Assignments[a]
υ(cm^{-1})	IR_I	R_A	υ(cm^{-1})	υ(cm^{-1})	–
3546	25.12	89.29	–	3505	υNH_2(100)
3446	84.42	600.55	3446	3464	υNH_2(99)
3086	7.26	140.72	3088	3102	υCHII(99)
3085	0.17	58.68	–	–	υCHII(100)
3077	1.53	91.04	–	–	υCHI(94)
3076	2.71	27.74	–	–	υCHI(95)
3074	3.92	38.26	–	3072	υCHII(99)
3042	23.36	152.04	–	–	υCHI(94)
3041	13.15	130.43	3038	3035	υCHI(95)
3011	8.55	13.03	–	–	υCH_3(57), υCH_2(42)
2992	0.11	68.35	–	–	υCH_3(27), υCH_2(63)
2988	9.81	100.21	2980	2978	υCH_3(98)
2944	7.84	72.02	2942	2940	υCH_2(98)
2925	25.45	257.58	–	–	υCH_3(100)
1601	349.65	365.92	1603	1608	δNH_2(61), υPhI(12)
1588	193.57	1466.99	–	–	δNH_2(10), υPhII(14), υPhI(50)
1583	12.76	113.63	–	–	δNH_2(14), υPhII(22), υPhI(47)
1575	30.26	1067.84	1571	–	υPhII(56), υPhI(22)
1544	18.69	387.49	1550	1550	υPhI(51), υPhII(19)
1526	128.59	3082.89	1515	–	υC = N(48), υPhII(41)
1474	353.91	379.48	1469	1467	υC = N(12), υPhI(54), δCHI(30)
1449	8.04	5.70	1444	1445	δCH_3(96)
1434	7.97	9.77	–	–	δCH_3(97)
1423	22.17	157.49	1425	1426	υPhII(68), δCHII(10)
1414	35.61	106.72	–	–	υPhI(53), δCHI(24)
1399	2.83	19.57	–	–	δCH_2(92)
1397	87.09	641.88	–	–	υPhII(59), υCNII(14), δCHII(14)
1358	1.11	0.48	1355	–	δCH_3(93)
1328	8.52	50.86	1326	1326	υPhII(71), δCH_3(11)
1310	0.98	24.94	–	–	υPhI(66), δNH_2(10)
1291	32.68	141.90	1294	1288	δCHI(43), υPhI(16)
1270	137.41	15.56	–	–	υCN(51), υPhI(21), δCHI(12)
1256	13.88	0.93	1260	1262	υC = N(13), δCHI(15), υPhI(14), υPhII(11)
1251	0.52	8.28	–	–	δCH_2(80)
1237	42.17	20.55	1236	1240	δCH_2(20), υSO_2(48), δCHII(12)
1228	89.54	128.29	–	–	δCH_2(14), δCHII(48), τPhII(14)
1209	168.13	1227.27	1211	1208	υCNII(57), δCHII(21)
1198	91.63	3.30	–	–	δCH_2(47), υSO_2(48)
1172	1.19	14.07	1173	1174	υCO(40), δCHII(44)
1154	166.80	379.50	1145	1148	δCHI(66), δCHII(18)
1110	6.80	6.71	1115	–	δCHI(64), υPhI(20)
1098	12.38	5.95	–	–	δCHII(46), υPhII(43)
1058	238.04	42.15	1062	1052	δCH_2(65), δCHII(20)
1031	22.20	3.91	1035	–	δCHI(45), δNH_2(40)
1026	10.28	9.63	–	–	υCC(40), δCH_3(47)
1018	28.92	4.52	–	–	υSO_2(17), υCO(10), δCH_2(20), δCH_3(27)
1016	17.81	5.19	–	–	δCH_2(26), δCH_3(47)
1010	48.93	11.15	1010	–	υCO(15), υPhII(41), δCHII(14)
981	13.85	4.57	978	–	δPhI(54), υPhI(19)
945	0.15	0.07	947	–	γCHI(85)
940	6.00	5.62	938	–	υCC(53), δCH_3(29)
928	0.38	0.65	–	–	γCHI(78), τPhI(14)
925	0.61	0.54	922	920	γCHII(87)
898	4.83	911.98	–	–	δPhII(49), υCN(12), υCS(10)
893	25.86	199.38	890	888	δPhIII(40), υCO(47)
874	9.23	3.29	–	–	γCHII(79), τPhII(10)
816	14.10	11.91	820	820	γCHI(55), υPhI(17)
811	33.78	1.09	808	–	γCHI(51), γCN(12)
797	17.64	19.96	–	–	γCHII(60), υPhI(12)
793	24.79	33.22	–	–	γCHII(66), υPhI(10)
792	5.21	2.95	788	–	υPhI(92)
758	4.09	0.10	753	–	δCH_2(61), δCH_3(32)
731	1.00	0.98	–	735	τPhII(50), τPhIII(33)
724	14.64	3.46	–	–	τPhI(31), γCC(37), τPhIII(15), τPhII(10)
699	93.03	14.15	695	696	δPhIII(18), υCS(45), δPhII(13)
684	7.84	0.33	–	–	τPhI(47), τPhIII(15), γCN(19)
655	56.02	16.99	–	–	υCS(48), δPhIII(10)
631	2.24	3.19	633	635	δPhII(26), δPhI(24), γNH_2(35)
627	1.94	7.95	–	–	δPhI(72)
587	10.18	9.13	590	591	τPhII(47), γCS(32)
577	76.59	3.34	566	–	δSO_2(39), δPhIII(28)
535	60.74	9.36	–	534	δSO_2(24), δPhII(23), δPhIII(14)
530	4.55	3.72	528	–	δPhII(40), δPhI(16), δPhIII(11)

(*continued on next page*)

Table 3 (*continued*)

B3LYP/6-311++G(d,p) (5D, 7F)			IR	Raman	Assignments[a]
υ(cm^{-1})	IR_I	R_A	υ(cm^{-1})	υ(cm^{-1})	–
505	19.77	3.05	498	504	γCN(31), τPhI(28), γCC(20)
451	27.33	5.7	455	448	δSO_2(63), τPhII(20)
436	437.39	67.75	438	–	γCN(80)
422	46.37	6.49	–	–	τPhII(51), τPhIII(24)
414	0.88	1.00	413	–	δSO_2(22), δCN(19), δCS(13), δCC(10)
402	0.24	0.07	403	–	τPhI(81)
379	7.65	3.71	–	–	τPhIII(18), τPhII(11), δSO_2(36)
373	0.07	0.83	–	–	δSO_2(23), δCN(43)
342	14.47	0.12	–	–	τNH_2(92)
328	13.17	1.23	–	329	τPhII(20), δSO_2(42), τPhI(10)
308	0.47	1.82	–	–	δSO_2(47)
307	3.31	4.87	–	–	γCS(19), δPhI(18), γCC(10)
269	0.19	0.54	–	270	δSO_2(50), δCC(12)
254	9.39	3.01	–	–	δCH_2(25), δSO_2(18), γCC(10)
246	3.73	0.98	–	–	τPhII(45), τPhIII(18)
195	0.99	4.34	–	–	δCH_2(10), δSO_2(25)
191	0.21	0.60	–	–	δSO_2(12), τCH_3(69)
179	2.30	1.94	–	168	τPhII(18), δSO_2(23), δCH_2(14), τPhI(12)
144	1.29	2.20	–	–	δCS(45), δCC(12), δSO_2(10)
123	1.53	1.82	–	–	τPhI(33), δSO_2(21), τPhIII(11)
71	0.82	0.54	–	–	τCH_2(32), δPhII(20), δCC(16)
68	0.57	0.91	–	–	γCS(26), δSO_2(23), τCC(14)
55	0.98	0.54	–	–	τCH_2(26), τSO_2(28), τCC(18)
50	1.01	0.27	–	–	τCH_2(23), τCC(45)
32	1.86	5.47	–	–	τSO_2(28), τCC(41)
24	2.63	3.03	–	–	τSO_2(45), γCC(12)

[a] υ-stretching; δ-in-plane deformation; γ-out-of-plane deformation; τ-torsion; PhI-Para substituted phenyl ring; PhII-tri-substituted phenyl ring; PhIII-benzoxazole ring; potential energy distribution is given in brackets in the assignment column; IR_I-IR intentity; R_A-Raman activity; Potential energy distribution in % is given in brackets in the assignment column.

with higher energies, −0.26950, −0.26887, −0.34202a.u and considerable p-characters, 99.82, 99.83, 100% and low occupation numbers, 1.79080, 1.78931, 1.73225. The lower energy orbitals are: $n_1(O_{11})$, $n_1(O_{12})$, $n_1(O_{21})$ with lower energy orbitals, −0.76539, −0.76505, −0.59498a.u with p-characters, 25.39, 25.37, 62.31% and high occupation numbers, 1.98235, 1.98234, 1.96957.

Thus, a very close to pure p-type lone pair orbital participates in the electron donation to the $n_3(O_{11}) \rightarrow \sigma^*(S_{10}-O_{12})$, $n_3(O_{12}) \rightarrow \sigma^*(S_{10}-O_{11})$, $n_1(N_{20}) \rightarrow \sigma^*(O_{21}-C_{22})$, $n_2(O_{21}) \rightarrow \pi^*(N_{20}-C_{22})$ and C_{28} of $n_1(C_{28}) \rightarrow \pi^*(N_{20}-C_{22})$ interactions in the compound. The results are tabulated in Table 5.

6.4. Nonlinear optical properties

NLO techniques are considered as one among the most structure sensitive method to study molecular structure and assemblies since the potential or organic materials for NLO device have been proven. For the title compound the first order hyperpolarizability is 31.19×10^{-30} which comparable with the reported values of similar derivatives [34] and which is 239.92 times that of the standard NLO material urea (0.13×10^{-30}) [35]. We conclude that the title compound is an attractive object for future studies of nonlinear optics. The high value of hyperpolarizability may be due to π-electron cloud movement from donor to acceptor which makes the molecule highly polarized and the intra-molecular charge transfer. The theoretical second order hyperpolarizability was calculated using the Gaussian 09 software and is equal to -22.127×10^{-37} esu [36].

6.5. Molecular electrostatic potential (MEP)

MEP is related to the electron density and is a very useful descriptor in understanding sites for electrophilic and nucleophilic reactions [37,38]. To predict reactive sites of electrophilic and nucleophilic attacks for the title compound, MEP at the B3LYP/6-311++G(d,p) (5D, 7F) optimized geometry was calculated. The negative (red and yellow) regions of MEP were related to electrophilic reactivity and the positive (blue) regions to nucleophilic reactivity (Fig. 4). From MEP it is evident that the negative charge covers the O atoms of SO_2 group, N atom of benzoxazole group and the positive region is over the NH_2 group.

6.6. Frontier molecular orbital analysis

It is important that ionization potential (I), electron affinity (A), electrophilicity index (ω), chemical potential (μ), electronegativity (χ) and hardness (η) to be put into a molecular orbital frame work. Based on density functional descriptors, global chemical reactivity descriptors of compounds such as hardness, chemical potential, softness, electro negativity and electrophilicity index as well as local reactivity has been defined [39,40]. Using Koopman's theorem for closed shell components η, μ and χ can be defined as $\eta = (I-A)/2$; $\mu = -(I + A)/2$; $\chi = (I + A)/2$; where I and A are the ionization potential and electron affinity, respectively. The ionization energy (I) and electron affinity (A) can be expressed through HOMO and LUMO orbital energies as $I = -E_{HOMO} = 8.155$ and $A = -E_{LUMO} = 4.5994$ eV. Electron affinity refers to the capability of ligand to accept precisely one electron from a donor. However, in many kinds of bonding viz. covalent hydrogen bonding, partial charge transfer takes place. Considering the chemical hardness (η), large HOMO-LUMO energy gap means a hard molecule and small HOMO-LUMO gap means a soft molecule. One can also relate the stability of the molecule to hardness, which means that the molecule with smaller HOMO-LUMO gap is more reactive. For the title compound, the energy gap is 3.161 eV. Parr et al. [39] have defined a new descriptor to quantity the global electrophilic power of the compound as electrophilicity index (ω) which defines a quantitative classification of global electrophilic nature of a compound. Parr et al. have proposed electrophilicity index (ω) as a measure of energy lowering due to maximal electron flow between donor and

Table 4
Second-order perturbation theory analysis of Fock matrix in NBO basis corresponding to the intramolecular bonds of the title compound.

Donor(i)	Type	ED/e	Acceptor(j)	Type	ED/e	E(2)[a]	E(j)-E(i)[b]	F(i,j)[c]
C2–C3	σ	1.97639	C1–C2	σ*	0.02459	3.54	1.28	0.060
_	–	–	C3–C4	σ*	0.02124	4.33	1.28	0.066
_	–	–	C22–C28	σ*	0.03419	1.41	1.20	0.037
_	π	1.58238	C1–C6	π*	0.37491	21.94	0.28	0.071
_	–	–	C4–C5	π*	0.32922	18.30	0.29	0.066
_	–	–	N20–C22	π*	0.31817	10.42	0.28	0.049
C6–S10	σ	1.96654	C1–C2	σ*	0.02459	2.42	1.25	0.049
_	–	–	C4–C5	σ*	0.01422	2.47	1.24	0.050
_	–	–	S10–O11	σ*	0.14715	3.25	0.96	0.051
_	–	–	S10–O12	σ*	0.14669	3.22	0.96	0.051
_	–	–	S10–C13	σ*	0.20293	1.36	0.81	0.031
_	–	–	C13–C16	σ*	0.00681	1.17	1.04	0.031
S10–O11	σ	1.98580	C6–S10	σ*	0.20578	1.09	1.11	0.033
_	–	–	S10–O12	σ*	0.14669	2.15	1.24	0.048
_	–	–	S10–C13	σ*	0.20293	1.28	1.08	0.035
S10–O12	σ	1.98577	C6–S10	σ*	0.20578	1.07	1.11	0.032
_	–	–	S10–O11	σ*	0.14715	2.15	1.24	0.048
_	–	–	S10–C13	σ*	0.20293	1.29	1.08	0.035
S10–C13	σ	1.96806	C1–C6	σ*	0.02068	1.42	0.66	0.030
_	–	–	C6–S10	σ*	0.20578	1.32	0.81	0.031
_	–	–	S10–O11	σ*	0.14715	3.31	0.93	0.051
_	–	–	S10–O12	σ*	0.14669	3.32	0.94	0.051
N20–C22	σ	1.98546	C1–C2	σ*	0.02459	5.94	1.45	0.083
_	–	–	C2–N20	σ*	0.02003	1.01	1.33	0.033
_	–	–	C22–C28	σ*	0.03419	2.95	1.37	0.057
_	–	–	C27–C28	σ*	0.03419	1.48	1.44	0.041
_	π	1.86000	C2–C3	π*	0.45060	16.74	0.34	0.073
O21–C22	σ	1.98855	C3–C4	σ*	0.02124	5.04	1.46	0.077
_	–	–	C23–C28	σ*	0.02176	1.66	1.45	0.044
LPO11	σ	1.98235	S10–O12	σ*	0.14669	1.47	1.06	0.036
_	π	1.82204	C6–S10	σ*	0.20578	12.63	0.44	0.067
_	–	–	S10–C13	σ*	0.20293	16.54	0.41	0.074
_	n	1.79080	C6–S10	σ*	0.20578	7.58	0.43	0.051
_	–	–	S10–O12	σ*	0.14669	22.80	0.56	0.102
_	–	–	S10–C13	σ*	0.20293	3.39	0.40	0.033
LPO12	σ	1.98234	S10–O11	σ*	0.14715	1.48	1.05	0.036
_	π	1.82161	C6–S10	σ*	0.20578	12.49	0.44	0.066
_	–	–	S10–C13	σ*	0.20293	16.76	0.40	0.074
_	n	1.78931	C6–S10	σ*	0.20578	7.85	0.43	0.052
_	–	–	S10–O11	σ*	0.14715	22.87	0.56	0.102
_	–	–	S10–C13	σ*	0.20293	3.23	0.40	0.032
LPN20	σ	1.90908	C2–C3	σ*	0.04247	6.36	0.90	0.068
_	–	–	O21–C22	σ*	0.06464	14.48	0.68	0.089
LPO21	σ	1.96957	C2–C3	σ*	0.04247	3.69	1.13	0.058
_	–	–	N20–C22	σ*	0.01724	4.82	1.17	0.067
_	π	1.73225	C2–C3	π*	0.45060	25.37	0.36	0.089
_	–	–	N20–C22	π*	0.31817	32.94	0.35	0.097
LPC28	σ	1.09923	N20–C22	π*	0.31817	79.88	0.12	0.104
_	–	–	C23–C24	π*	0.29425	70.01	0.15	0.108
_	–	–	C26–C27	π*	0.31306	73.54	0.14	0.109

[a] E(2) means energy of hyper-conjugative interactions (stabilization energy in kJ/mol).
[b] Energy difference (a.u) between donor and acceptor i and j NBO orbitals.
[c] F(i,j) is the Fock matrix elements (a.u) between i and j NBO orbitals.

acceptor. They defined electrophilicity index as follows: $\omega = \mu^2/2\eta$. The usefulness of this new reactivity measure has been recently demonstrated in understanding the toxicity of various pollutants in terms of their reactivity and site selectivity [41]. The calculated values of ω, μ, χ and η are 13.672, −6.575, 6.575 and 1.581 eV respectively. The calculated value of electrophilicity index describes the biological activity of the title compound. The atomic orbital components of the frontier molecular orbital are shown in Fig. 5.

6.7. Geometrical parameters

The optimized molecular structure of the title compound was determined by using Gaussian 09 program and the optimized geometry is summarized in Table 1. From the table, the C–C bond length C_2–C_3 (1.4026 Å) is greater than that of C_3–C_4 (1.3838 Å) and C_2–C_1 (1.3933 Å), because of the delocalization of electron density of C_2–C_3 with the phenyl ring. Also C_3–O_{21} (1.3653 Å),

Table 5
NBO results showing the formation of Lewis and non-Lewis orbitals.

Bond(A-B)	ED/e[a]	EDA%	EDB%	NBO	s%	p%
σ C2–C3	1.97639	49.78	50.22	0.7056($sp^{2.11}$)C+	32.09	67.91
_	−0.70353	–	–	0.7086($sp^{1.83}$)C	35.29	64.71
π C2–C3	1.58238	50.86	49.14	0.7131($sp^{1.00}$)C+	0.00	100.0
_	−0.26742	–	–	0.7010($sp^{1.00}$)C	0.00	100.0
σ C6–S10	1.96654	54.34	45.66	0.7371($sp^{3.16}$)C+	24.01	75.99
_	−0.67132	–	–	0.6757($sp^{3.11}$)S	24.03	75.97
σ S10–O11	1.98580	33.80	66.20	0.5814($sp^{2.75}$)S+	26.32	73.68
_	−0.94866	–	–	0.8137($sp^{2.95}$)O	25.18	74.82
σ S10–O12	1.98577	33.82	66.18	0.5815($sp^{2.74}$)S+	26.37	73.63
_	−0.94904	–	–	0.8135($sp^{2.96}$)O	25.17	74.83
σ S10–C13	1.96806	47.55	52.45	0.6896($sp^{3.16}$)S+	23.72	76.28
_	−0.64563	–	–	0.7242($sp^{4.16}$)C	19.36	80.64
σ N20–C22	1.98546	58.82	41.18	0.7669($sp^{1.73}$)N+	36.54	63.46
_	−0.86996	–	–	0.6418($sp^{1.81}$)C	35.63	64.37
π N20–C22	1.86000	60.35	39.65	0.7768($sp^{1.00}$)N+	0.00	100.0
_	−0.32216	–	–	0.6297($sp^{1.00}$)C	0.00	100.0
σ O21–C22	1.98855	69.41	30.59	0.8331($sp^{2.30}$)O+	30.27	69.73
_	−0.88969	–	–	0.5531($sp^{3.04}$)C	24.68	75.32
n1O11	1.98235	–	–	$sp^{0.34}$	74.61	25.39
_	−0.76539	–	–	–	–	–
n2O11	1.82204	–	–	$sp^{1.00}$	0.01	99.99
_	−0.27052	–	–	–	–	–
n3O11	1.79080	–	–	$sp^{99.99}$	0.18	99.82
_	−0.26950	–	–	–	–	–
n1O12	1.98234	–	–	$sp^{0.34}$	74.63	25.37
_	−0.76505	–	–	–	–	–
n2O12	1.82161	–	–	$sp^{99.99}$	0.01	99.99
_	−0.27001	–	–	–	–	–
n3O12	1.78931	–	–	$sp^{99.99}$	0.17	99.83
_	−0.26887	–	–	–	–	–
n1N20	1.90908	–	–	$sp^{2.11}$	32.12	67.88
_	−0.36850	–	–	–	–	–
n1O21	1.96957	–	–	$sp^{1.65}$	37.69	62.31
_	−0.59498	–	–	–	–	–
n2O21	1.73225	–	–	$sp^{1.00}$	0.00	100.0
_	−0.34202	–	–	–	–	–

[a] ED/e is expressed in a.u.

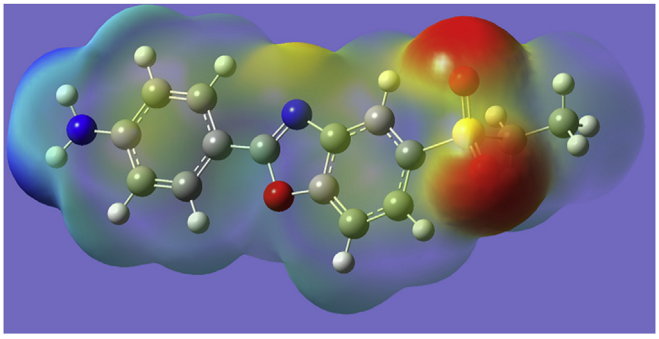

Fig. 4. MEP plot of 5-Ethylsulphonyl-2-(p-aminophenyl)benzoxazole.

C_{22}–O_{21} (1.3871 Å), C_2–N_{20} (1.3882 Å) and C_{22}–N_{20} (1.2988 Å) bond lengths are different because of the difference in their environment and also assume a double character in C_{22}–N_{20}. Hyperconjugation is the interaction of the electrons in a sigma bond (usually C–H or C–C) with an adjacent empty (or partially filled) non-bonding π-orbital, anti-bonding σ or π orbital, or filled π orbital to give an extended molecular orbital that increases the stability of the system. The bond angle C_{28}–C_{22}–O_{21} (117.4°) and C_{28}–C_{22}–N_{20} (128.3°) indicates the π bond character of the former [42,43]. Also C_3–O_{21}–C_{22} (104.5°) and C_2–N_{20}–C_{22} (105.0°)

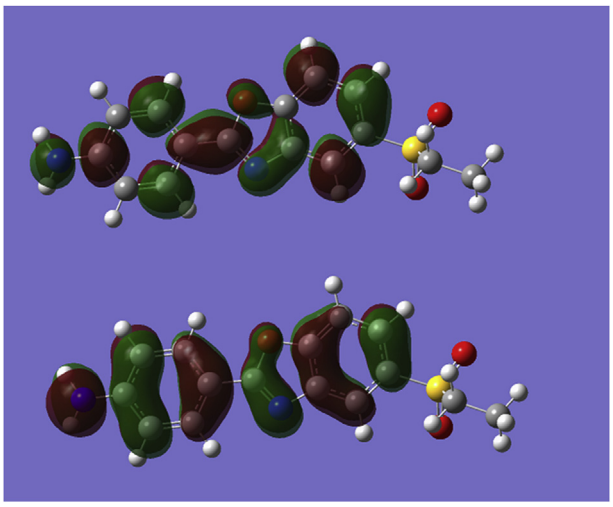

Fig. 5. HOMO-LUMO plots of 5-Ethylsulphonyl-2-(p-aminophenyl)benzoxazole.

indicates slightly higher electronegative property of oxygen atom [43]. Bond angles C_4–C_3–O_{21} (128.5) and C_1–C_2–N_{20} (131.4°) are higher than 120° indicates the presence of hyper-conjugation [26,44,45].

At C_{22} position, the bond angles C_{28}–C_{22}–O_{21} is reduced by 2.6° and C_{28}–C_{22}–N_{20} is increased by 8.3° from 120°, which indicates the interaction between O_{21} and H_{32}. For the title compound the bond lengths C_3–O_{21}, C_2–N_{20} are found to be 1.3653 and 1.3882 Å, which are in agreement with literature [43]. The ethylsulphonyl moiety is tilted from tri-substituted phenyl ring as is evident from the torsion angles C_2–C_1–C_6–S_{10} = 178.7, C_1–C_6–S_{10}–C_{13} = −88.6, C_4–C_5–C_6–S_{10} = −179.0 and C_5–C_6–S_{10}–C_{13} = 90.9°. The aromatic ring of the title compound is somewhat irregular and the spread of C–C bond distance is 1.3954–1.4183 in PhI and 1.4016–1.4137 Å in PhII, which is similar to the spread reported by Bhagyasree et al. [43].

6.8. Molecular docking

PASS (Prediction of Activity Spectra) [46] is an online tool which predicts different types of activities based on the structure of a compound. PASS analysis of the 5-Ethylsulphonyl-2-(p-aminophenyl)benzoxazole predicts amongst other activities, Focal adhesion kinase 2 inhibitor activity with Pa (Probability to be active) value of 0.527 (Table 6). Focal adhesion kinase (FAK), a nonreceptor cytoplasmic protein tyrosine kinase, is a key regulator of signals from the extracellular matrix (ECM) mediated by integrins and growth factor receptors (GFR) [47]. FAK has been implicated in the regulation of a variety of cellular signalling pathways that control cell proliferation, cell-cycle progression, migration and cell survival [48–50]. To evaluate the inhibitory nature of the compound against FAK protein, molecular docking studies were carried out. The 3D crystal structure of FAK was obtained from Protein Data Bank (PDB ID: 4K9Y) [51] and 4K9Y has a good resolution (2 Å) and attached co-crystallized inhibitors were used to identify the active site. Molecular docking is an efficient tool to get an insight into ligand–receptor interactions. All molecular docking calculations were performed on AutoDock-Vina software [52] and the AutoDock Tools (ADT) graphical user interface was used to calculate Kollmann charges for the protein and to add polar hydrogen's. Water molecules and co-crystallized ligands were removed and the ligand was prepared for docking by minimizing its energy at B3LYP/6-311++G(d,p) (5D, 7F) level of theory. Partial charges were

Table 6
PASS prediction for the activity spectrum of the compound, Pa represents probability to be active and Pi represents probability to be inactive.

0.812	0.003	Muscular dystrophy treatment
0.527	0.006	Focal adhesion kinase 2 inhibitor
0.550	0.049	CYP3A2 substrate
0.508	0.012	Non-steroidal antiinflammatory agent
0.532	0.048	Antiinflammatory
0.489	0.006	Cyclooxygenase 1 inhibitor
0.538	0.060	Oxidoreductase inhibitor
0.496	0.050	CYP3A1 substrate
0.457	0.014	Linoleoyl-CoA desaturase inhibitor
0.451	0.019	Alzheimer's disease treatment
0.432	0.035	Antidiabetic
0.464	0.076	Anaphylatoxin receptor antagonist
0.392	0.024	Focal adhesion kinase inhibitor
0.362	0.002	D-Ala-D-Ala ligase inhibitor
0.375	0.017	Vascular (periferal) disease treatment
0.457	0.111	TP53 expression enhancer
0.380	0.037	Antituberculosis
0.375	0.046	Antimycobacterial
0.333	0.005	Vascular endothelial growth factor 3 antagonist
0.396	0.081	Antiarthritic
0.343	0.033	CYP2C6 substrate
0.429	0.123	Acute neurologic disorders treatment
0.420	0.116	Gastrin inhibitor
0.330	0.030	TRPA1 agonist
0.320	0.021	CYP2B2 substrate
0.363	0.066	Rhinitis treatment
0.299	0.006	Proto-oncogene tyrosine-protein kinase Fyn inhibitor
0.376	0.084	Neurodegenerative diseases treatment
0.316	0.025	Systemic lupus erythematosus treatment
0.299	0.009	Cyclooxygenase inhibitor
0.326	0.053	Antiinflammatory, intestinal
0.304	0.037	Myeloblastin inhibitor
0.280	0.014	Antileprosy
0.378	0.112	NADPH peroxidase inhibitor
0.314	0.049	Antineoplastic (pancreatic cancer)
0.356	0.092	Kinase inhibitor
0.281	0.020	Keratolytic
0.335	0.078	FMO1 substrate
0.322	0.067	Atherosclerosis treatment
0.311	0.058	Eye irritation, inactive

calculated by Geistenger method and torsion and rotatable bonds were defined. The active site of the enzyme was defined to include residues of the active site within the grid size of 40 Å × 40 Å × 40 Å. Lamarckian Genetic Algorithm (LGA) available in Auto Dock Vina was employed for docking. The docking protocol was tested by removing co-crystallized inhibitor from the protein and then docking it at the same site. To evaluate the quality of docking results, the common way is to calculate the Root Mean Square

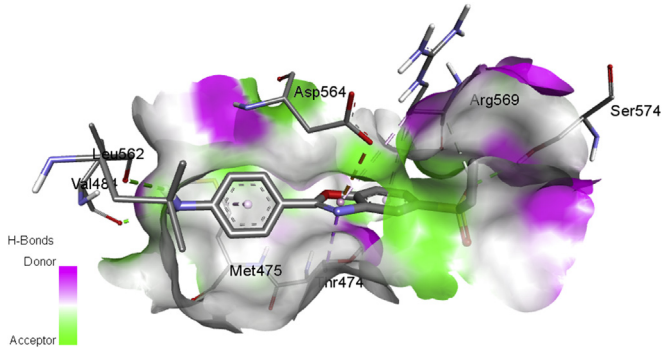

Fig. 6. The docked confirmation of ligand binds at the catalytic site of FAK. H-bond, alkyl-π and sigma-π interactions are represented by green, pink and violet dotted lines, respectively. Hydrogen bonding pocket is shown for clarity. (For interpretation of the references to colour in this figure legend, the reader is referred to the web version of this article.)

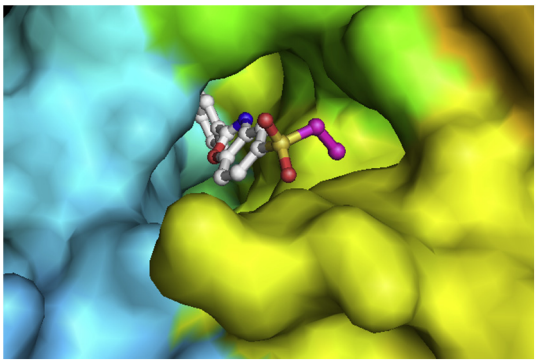

Fig. 7. Surface view of protein (FAK) with docked ligang embedded in the active site.

Deviation (RMSD) between the docked pose and the known crystal structure confirmation. RMSD values up to 2 Å are considered reliable for the docking protocol [53]. The docking protocol we employed predicted a similar confirmation with RMSD value well within the allowed range of 2 Å (Fig. 6). Amongst the docked confirmations of the title compound, the confirmation which was close to the confirmation of co-crystallized ligand scored well was visualized for ligand–protein interactions in Discover Studio Visualizer 4.0 and pymol software. The ligand binds at the active sites of the protein by weak non-covalent interactions most prominent of which are H-bonding, alkyl-π and sigma-π interactions. Amino acids viz. Ser574, Val484 and Leu 562 form H-bonds with the ligand (Fig. 7). The residues Arg569 and Met475 hold the phenyl rings of the compound by alkyl-π interactions. Thr 474 is involved in a sigma-π interaction with the ligand (Fig. 6). Binding free energy (ΔG in kcal/mol) of −9.8 as predicted by Autodock Vina (Table 7) suggests good binding affinity. The inhibitor forms a stable complex with FAK as is evident from the ligand–receptor interactions (Figs. 7 and 8).

7. Conclusion

Synthesis, antibacterial and antimicrobial activities of 5-Ethylsulphonyl-2-(p-aminophenyl)benzoxazole is reported. The molecular structural parameters and vibrational wavenumbers have been obtained using density functional theory. Detailed vibrational assignments of the observed IR and Raman bands have been proposed on the basis of potential energy distribution analysis and most of the modes have wavenumbers in the expected range. The molecular electrostatic potential has been mapped for predicting sites and relative reactivities towards electrophilic and nucleophilic attack. The first and second order hyperpolarizabilities are calculated and the first order hyperpolarizability is 239.92 times

Table 7
Binding affinity of different poses of the title compound as predicted by Autodock Vina.

Mode	Affinity	Distance from best mode	
–	(kcal/mol)	RMSD l.b	RMSD u.b.
1	−9.8	0.000	0.000
2	−9.6	2.554	2.213
3	−9.5	2.166	2.777
4	−7.2	11.324	13.411
5	−7.0	5.803	7.298
6	−6.9	11.551	13.505
7	−6.8	13.689	17.184
8	−6.8	20.271	22.502
9	−6.8	3.319	4.317

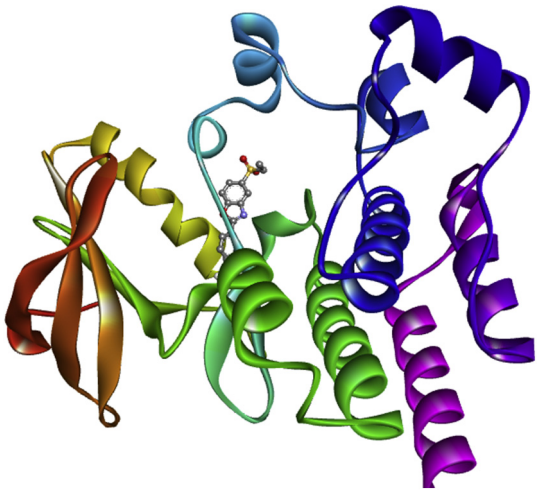

Fig. 8. The ligand and the co-crystallized inhibitor embedded into the active site of FAK.

that of the standard NLO material urea and hence the title compound and its derivatives are good objects for future studies of nonlinear optics. The title compound possessed lower activity against *C. albicans* with MIC value of 64 μg/ml than compared reference drugs as fluconazole and amphotericin B and on the other hand, it possessed the same activity with value of 64 μg/ml against *C. krusei* as the reference drug, fluconazole. PASS analysis of the title compound predicts amongst other activities, Focal adhesion kinase 2 inhibitor activity with probability active value of 0.527 and the binding free energy of −9.8 cal/mol as predicted by Autodock Vina suggests good binding affinity.

Acknowledgements

The authors would like to extend their sincere appreciation to the Deanship of Scientific Research at King Saud University for funding this work through the Research Group Project No. PRG-1436-23. The authors are thankful to University of Antwerp for access to the University's CalcUA Supercomputer Cluster.

References

[1] A.D. Rodriguez, C. Ramrez, I.I. Rodriguez, E. Gonzalez, Org. Lett. 1 (1999) 527.
[2] S.M. Rida, F.A. Ashour, S.A.M. El-Hawash, M.M. El-Semary, M.H. Badr, M.A. Shalaby, Eur. J. Chem. 40 (2005) 949.
[3] I. Yildiz-Oren, I. Yalcin, E. Aki-Sener, N. Ucarturk, Eur. J. Med. Chem. 39 (2004) 291.
[4] I. Yildiz-Oren, B. Tekiner-Gulbas, I. Yalcin, O. Temiz-Arpaci, E. Aki-Sener, N. Altanlar, Arch. Pharm. 337 (2004) 402.
[5] O. Temiz-Arpaci, A. Ozdemir, I. Yalcin, I. Yildiz, E. Aki-Sener, N. Altanlar, Arch. Pharm. 338 (2005) 105.
[6] A. Akbay, I. Oren, O. Temiz-Arpaci, E. Aki-Sener, I. Yalcin, Arzneim. Forsch 53 (2003) 266.
[7] R.K. Plemperm, K.J. Erlandson, A.S. Lakdawala, A. Sun, A. Prussia, J. Boonsombat, E. Aki-Sener, I. Yalcin, I. Yildiz, O. Temiz-Arpaci, B.P. Tekiner, D. Liotta, J.P. Snyder, Proc. Natl. Acad. Sci. U. S. A. 101 (2004) 5628.
[8] H. Lage, E. Aki-Sener, I. Yalcin, Int. J. Cancer 119 (2006) 213.
[9] A. Pinar, P. Yurdakul, I. Yilidiz, O. Temiz-Arpaci, N.L. Acan, E. Aki-Sener, I. Yalcin, Biochem. Biophys. Res. Commun. 317 (2004) 670.
[10] O. Temiz-Arpaci, B. Tekiner-Gulbas, I. Yildiz, E. Aki-Sener, I. Yalcin, Bioorg. Med. Chem. 13 (2005) 6354.
[11] B. Tekiner-Gulbas, O. Temiz-Arpaci, I. Yildiz, E. Aki-Sener, I. Yalcin, Sar. QSAR Environ. Res. 17 (2006) 121.
[12] P. Anusha, J.V. Rao, Int. J. Pharm. Biol. Sci. 4 (2014) 83.
[13] Y.S. Mary, K. Raju, I. Yildiz, O. Temiz-Arpaci, H.I.S. Nogueira, C.M. Garandeiro, C. Van Alsenoy, Spectrochim. Acta 96 (2012) 617.
[14] Y.S. Mary, K. Raju, T.E. Bolelli, I. Yildiz, H.I.S. Nogueira, C.M. Granadeiro, C. Van Alsenoy, J. Mol. Struct. 1012 (2012) 22.
[15] O. Temiz-Arpacı, B.E. Cıfcıoglu-Goztepe, F. Kaynak-Onurdag, S. Ozgen, F.S. Senol, I. Erdogan-Orhan, Acta Biol. Hung. 64 (2013) 249.
[16] C.L.S.I. (formerly NCCLS), Reference Method for Both Dilution Antifungal Susceptibility Testing Yeast, Approved Standard, 27-A3, Clinical and Laboratory Standards Institute, Wayne, PA, USA, 2006.
[17] C.L.S.I. (formerly NCCLS), Performance Standards for Antimicrobial Susceptibility Testing; 16th Informational Supplement, CLSI M100-S18, Clinical and Laboratory Standards Institute, Wayne, PA, USA, 2008.
[18] M.J. Frisch, G.W. Trucks, H.B. Schlegel, G.E. Scuseria, M.A. Robb, J.R. Cheeseman, G. Scalmani, V. Barone, B. Mennucci, G.A. Petersson, H. Nakatsuji, M. Caricato, X. Li, H.P. Hratchian, A.F. Izmaylov, J. Bloino, G. Zheng, J.L. Sonnenberg, M. Hada, M. Ehara, K. Toyota, R. Fukuda, J. Hasegawa, M. Ishida, T. Nakajima, Y. Honda, O. Kitao, H. Nakai, T. Vreven, J.A. Montgomery Jr., J.E. Peralta, F. Ogliaro, M. Bearpark, J.J. Heyd, E. Brothers, K.N. Kudin, V.N. Staroverov, T. Keith, R. Kobayashi, J. Normand, K. Raghavachari, A. Rendell, J.C. Burant, S.S. Iyengar, J. Tomasi, M. Cossi, N. Rega, J.M. Millam, M. Klene, J.E. Knox, J.B. Cross, V. Bakken, C. Adamo, J. Jaramillo, R. Gomperts, R.E. Stratmann, O. Yazyev, A.J. Austin, R. Cammi, C. Pomelli, J.W. Ochterski, R.L. Martin, K. Morokuma, V.G. Zakrzewski, G.A. Voth, P. Salvador, J.J. Dannenberg, S. Dapprich, A.D. Daniels, O. Farkas, J.B. Foresman, J.V. Ortiz, J. Cioslowski, D.J. Fox, Gaussian 09, Revision C.01, Gaussian, Inc., Wallingford CT, 2010.
[19] D.C. Young, Computational Chemistry: A Practical Guide for Applying Techniques to Real World Problems, John Wiley and Sons, Inc., New York.
[20] C.Y. Panicker, H.T. Varghese, P.S. Manjula, B.K. Sarojini, B. Narayana, J.A. War, S.K. Srivastava, C. Van Alsenoy, A.A. Al-Saadi, Spectrochim. Acta 151 (2015) 198.
[21] J.B. Foresman, in: E. Frisch (Ed.), Exploring Chemistry with Electronic Structure Methods, A Guide to Using Gaussian, Pittsburg, PA, 1996.
[22] R. Dennington, T. Keith, J. Millam, Gaussview, Version 5, Semichem. Inc., Shawnee Missions, KS, 2009.
[23] J.M.L. Martin, C. Van Alsenoy, GAR2PED, A Program to Obtain A Potential Energy Distribution from a Gaussian Archive Record, University of Antwerp, Belgium, 2007.
[24] N.P.G. Roeges, A Guide to the Complete Interpretation of Infrared Spectra of Organic Structures, John Wiley and Sons Inc., New York, 1994.
[25] N.B. Colthup, L.H. Daly, S.E. Wiberly, Introduction to Infrared and Raman Spectroscopy, third ed., Academic Press, Boston, 1990.
[26] J.B. Bhagyasree, J. Samuel, H.T. Varghese, C.Y. Panicker, M. Arisoy, O. Temiz-Arpaci, Spectrochim. Acta 115 (2013) 79.
[27] R.M. Silverstein, G.C. Bassler, T.C. Morril, Spectrometric Identification of Organic Compounds, fifth ed., John Wiley and Sons Inc., Singapore, 1991.
[28] P.L. Anto, C.Y. Panicker, H.T. Varghese, D. Philip, O. Temiz-Arpaci, B. Tekiner-Gulbas, I. Yildiz, Spectrochim. Acta 67 (2007) 744.
[29] C.Y. Panicker, H.T. Varghese, K.M. Pillai, Y.S. Mary, K. Raju, T.K. Manojkumar, A. Bielenica, C. Van Alsenoy, Spectrochim. Acta 75 (2010) 1559.
[30] G. Varsanyi, Assignments of Vibrational Spectra of Seven Hundred Benzene Derivatives, Wiley, New York, 1974.
[31] Y.S. Mary, H.T. Varghese, C.Y. Panicker, T. Ertan, I. Yildiz, O. Temiz-Arpaci, Spectrochim. Acta 71 (2008) 566.
[32] A.R. Ambujakshan, V.S. Madhavan, H.T. Varghese, C.Y. Panicker, O. Temiz-Arpaci, B.T. Gulbas, I. Yildiz, Spectrochim. Acta 69 (2007) 782.
[33] E.D. Glendening, A.E. Reed, J.E. Carpenter, F. Weinhold, NBO Version 3.1, Gaussian Inc., Pittsburgh, PA, 2003.
[34] L.N. Kuleshova, M.Y. Antipin, V.N. Khrustalev, D.V. Gusev, E.S. Bobrikova, Kristallografiya 48 (2003) 594–601.
[35] C. Adant, M. Dupuis, J.L. Bredas, Int. J. Quantum Chem. 56 (1995) 497.
[36] G. Mahalakshmi, V. Balachandran, Spectrochim. Acta 131 (2014) 587.
[37] E. Scrocco, J. Tomasi, Adv. Quantum Chem. 11 (1978) 115.
[38] F.J. Luque, J.M. Lopez, M. Orozco, Theor. Chem. Acc. 103 (2000) 343.
[39] R.G. Parr, R.A. Donnelly, M. Levy, W.E. Palke, J. Chem. Phys. 68 (1978) 3801.
[40] P.K. Chattaraj, B. Maiti, U. Sarbar, J. Phys. Chem. A 107 (2003) 4973.
[41] R. Parthasarathi, J. Padmanabhan, V. Subramanian, B. Maiti, P.K. Chattaraj, J. Phys. Chem. 107 (2003) 10346.
[42] J.B. Bhagyasree, H.T. Varghese, C.Y. Panicker, J. Samuel, C. Van Alsenoy, S. Yilmaz, I. Yildiz, E. Aki, J. Mol. Struct. 1046 (2013) 92.
[43] J.B. Bhagyasree, H.T. Varghese, C.Y. Panicker, J. Samuel, C. Van Alsenoy, K. Bolelli, I. Yildiz, E. Aki, Spectrochim. Acta 102 (2013) 99.
[44] J.B. Bhagyasree, H.T. Varghese, C.Y. Panicker, J. Samuel, C. Van Alsenoy, T. Ertan-Bolelli, I. Yildiz, J. Mol. Struct. 1063 (2014) 16.
[45] I. Fernandez, G. Frenking, Chem. Eur. J. 12 (2006) 3617.
[46] A. Lagunin, A. Stepanchikova, D. Filimonov, V. Poroikov, Bioinformatics 16645 (2000) 747.
[47] M.D. Schaller, C.A. Borgman, B.S. Cobb, R.R. Vines, A.B. Reynolds, J.T. Parsons, Proc. Natl. Acad. Sci. U. S. A. 89 (1992) 5192.
[48] V. Golubovskaya, L. Beviglia, L.H. Xu, H.S. Earp, R. Crraven, W. Cance, J. Biol. Chem. 277 (2002) 38978.
[49] M.D. Schaller, Biochim. Biophys. Acta 1540 (2001) 1.
[50] J.T. Parsons, J. Cell Sci. 116 (2003) 1409.
[51] U. Gradler, J. Bomke, D. Musil, V. Dresing, M. Lehmann, G. Holzemann, H. Greiner, C. Esdar, M. Krier, T. Heinrich, Bioorg. Med. Chem. Lett. 23 (2013) 5401.
[52] O. Trott, A.J. Olson, J. Comput. Chem. 31 (2010) 455.
[53] B. Kramer, M. Rarey, T. Lengauer, Proteins Struct. Funct. Genet. 37 (1999) 228.